

Solid-State Forms of β -Resorcylic Acid: How Exhaustive should a Polymorph Screen be?

Solid-State Forms of β -Resorcylic Acid:
How Exhaustive should a Polymorph Screen be?

*Doris E. Braun, Panagiotis G. Karamertzanis, Jean-Baptiste Arlin, Alastair J. Florence,
Volker Kahlenberg, Derek A. Tocher, Ulrich. J. Griesser and Sarah L. Price*

Electronic Supporting Information

1 EXPERIMENTAL	3
1.1 Manual crystallization screen	3
1.2 Thermal analysis, thermodynamic and kinetic stability	7
1.3 X-ray diffractometry	8
2 THEORETICAL	12
2.1 Conformational analysis of βRA and the choice of method for ΔE_{intra}	12
2.2 Testing the model for the intermolecular forces for U_{inter}	15
2.3 Modeling of form I	18
2.4 Computational generation of the crystal energy landscape (CSP)	21

Solid-State Forms of β -Resorcylic Acid: How Exhaustive should a Polymorph Screen be?

1 EXPERIMENTAL

1.1 Manual crystallization screen

Tables S1 – S5 list the results from the manual polymorphism screen.

Table S1. Results: evaporation experiments^a (II° – form II°, I - form II, HH – hemihydrate, S_{AA} – acetic acid monosolvate, S_{DX} – dioxane hemisolvate, S_{DMSO} – dimethyl sulphoxide hemisolvate).

Solvent	Description	Form
<i>n</i> -Butanol	Needles and plates	II°, I
<i>i</i> -Butanol	Needles and plates	II°, I
<i>n</i> -Propanol	Needles and plates	II°, I
<i>i</i> -Propanol	Needles and plates	II°, I
Ethanol	Needles and plates	II°, I
Methanol	Some of the crystals (needles) turn opaque on heating <100°C (hydrate), needles and plates	HH, II°, I
Acetic acid	Needles, dehydrated/ desolvated crystals (pseudomorphosis)	II°, S _{AA}
Acetone	Needles and plates	II°, I
Acetonitrile	Mainly needles, few platy crystals	II°, I
Chloroform	Needles	II°
Diethyl ether	Needles and few plates	II°, I
Diisopropyl ether	Needles	II°
Dioxane	Needles and few plates; some crystals showed pseudomorphosis, indicating the presence of a desolvated form.	II°, I, (S _{DX})
Dimethyl formamide	Needles and plates	I, II°
Dimethyl sulphoxide	After 2 months crystallization of spherulithes (darken upon heating,)	S _{DMSO}
Ethyl methyl ketone	Hydrate (big, rectangular plates, desolvation ~90°C), needles and few plates	II°, HH, I
Ethyl acetate	Needles and plates	II°, I
Nitromethane	Needles and plates	II°, I
Pyridine	Solution turned yellow, light yellow crystals melt between 150 and 158 °C	Salt
Tetrahydrofuran	Needles	II°
Water	Repeated several times: in some experiments HH was obtained, in others mixtures of HH and form II°	HH, II°

^aA saturated solution (at RT) of β RA was filtrated and the solvent was evaporated from a watch glass at RT.

Solid-State Forms of β -Resorcylic Acid: How Exhaustive should a Polymorph Screen be?

Table S2. Results: crystallization experiments^a (II° – form II°, I - form I, HH – hemihydrate, MH – monohydrate, S_{DMF-I} and S_{DMF-II} – dimethyl formamide solvates).

Solvent	Method	Description	Form
<i>n</i> -Butanol	F/S	Needles	II°
<i>i</i> -Butanol	F/S	Mixture of forms II° and I	II°, I
<i>n</i> -Propanol	F	Plates and needles	II°, I
	S	Needles	II°
<i>i</i> -Propanol	F/S	Needles	II°
Ethanol	F/S	Needles and plates	II°, I
Methanol	F/S	Needles	II°
Acetic acid	F	Experiment repeated several times: unstable acetic acid solvate (dark crystals); however some of the clear crystals corresponded to form II°	II°, S _{AC}
	S	Needles	II°
Acetone	F	Rectangular plates and needles	HH, II°
	S	Needles	II°
Acetonitrile	F/S	Needles	II°
Diethyl ether	F/S	Needles and plates (part of the solvent evaporated)	II°, I
Diisopropyl ether	F/S	Needles and plates (part of the solvent evaporated)	II°, I
Dioxane	F/S	Needles	II°
Dimethyl formamide	F	Small crystals, which desolvated after removing form the mother liquor	S _{DMF-I} and S _{DMF-II}
Dimethyl sulphoxide	S	Needles and plates	II°, I
Ethyl methyl ketone	F/S	Blocks	S _{DMSO}
Ethyl acetate	F/S	Needles	II°
Dimethyl formamide	F/S	Needles	II°
Nitromethane	F	Needles	II°, I
	S	Needles	II°
Pyridine	F/S	Light yellow crystals	Salt
Tetrahydrofuran	F	Needles and plates	II°, I
	S	Needles	II°
Water	F	Very thin needles, desolvation ~50°C	MH
	S	Desolvation ~90°C, at higher temperatures than MH	HH

^aA hot saturated solution (close to the boiling point of each used solvent) was either cooled fast (F, in ice) or slow (S, test tube wrapped in aluminum foil) to 0° or RT, respectively.

Solid-State Forms of β -Resorcylic Acid: How Exhaustive should a Polymorph Screen be?

Table S3. Results: Precipitation experiments^a (DCM – dichloromethane, CH – cyclohexane, Tol – toluene, II° – form II, I – form I, HH – hemihydrate, S_{DX} – dioxane hemisolvate and S_{AA} – acetic acid monosolvate).

1 st Solvent	2 nd solvent	Description (HTM)	Form
<i>n</i> -Butanol	DCM	Needles	II°
	CH	Needles	II°
	Tol	Needles	II°
<i>i</i> -Butanol	DCM	Needles	II°
	CH	Form II° and I	II°, I
	Tol	Plates	I, II°
<i>n</i> -Propanol	DCM	Needles	II°
	CH	Needles	II°
	Tol	Small platy crystals	I, (II°)
<i>i</i> -Propanol	DCM	Needles	II°
	CH	Needles	II°
	Tol	Needles and plates	II°, I
Ethanol	DCM	Needles	II°
	CH	Needles, small plates and bigger rectangular plates	II°, I, HH
	Tol	Needles and plates	II°, I
Methanol	DCM	Needles and plates	II°, I
Acetic acid	DCM	Needles and plates	II°, I
	CH	Needles	II°
	Tol	Part of the crystals desolvated (S _{AC}), needles dehydrate at ~90°C	S _{AA} , HH
Acetone	DCM	Needles and plates	II°, I
	CH	Needles	II°
	Tol	Needles and plates	II°, I
Acetonitrile	DCM	Needles	II°
	Tol	Needles and plates	II°, I
	DCM	Needles	II°
Chloroform	DCM	Needles	II°
Diethyl ether	DCM	Needles and plates	I, II°
	CH	Needles	II°
	Tol	Needles and plates	I, II°
Diisopropyl ether	DCM	Needles	II°
	CH	Needles	II°
	Tol	Needles	II°
Dioxane	DCM	Different crystal forms	II°, I, HH
	CH	Desolvation (?) and dehydration	(S _{DX}), HH
	Tol	Needles and plates	II°, I
Ethyl methyl ketone	DCM	Needles	II°
	CH	Needles and plates	II°, I
	Tol	Needles and plates	II°, I
Ethylacetate	DCM	Needles and plates	II°, I
	CH	Dehydration (HH) and form II° (thinner needles)	HH, II°
	Tol	Needles and plates	II°, I
Nitromethane	DCM	Needles	II°
	CH	Needles and few plates	II°, I
Pyridine	DCM	Yellow, melts at 154°C, embedded in silicon oil: after melting solvent escapes	Salt
Tetrahydrofuran	DCM	Long thin needles	II°
	CH	Needles and platy crystals	HH, II°, I
	Tol	Needles and plates	II°, I
Water	Tol	Rectangular plates	HH

^aA Saturated solution (at RT) of β RA was prepared in solvent 1 and after filtration ca. three times the amount of solvent 2 was added.

Solid-State Forms of β -Resorcylic Acid: How Exhaustive should a Polymorph Screen be?

Table S4. Results: solvent mediated transformation experiments^a (II° - form II°, HH – hemihydrate, S_{DX} – dioxane hemisolvate, S_{DMF-II} – DMF ¾ solvate, S_{DMSO-II} – dimethyl sulphoxide hemisolvate).

Solvent	Form	Solvent	Form
<i>n</i> -Butanol	II°	Dioxane	S _{DX}
<i>i</i> -Butanol	II°	Dimethyl formamide	S _{DMF-II}
<i>n</i> -Propanol	HH	Dimethyl sulphoxide	S _{DMSO}
<i>i</i> -Propanol	II°	Ethyl methyl ketone	II°
Ethanol	II°	Ethylacetate	HH
Methanol	II°	Nitromethane	II°
Acetic acid	II°	Pyridine	Pyridinium-Salt
Acetone	II°	Tetrahydrofurane	HH
Acetonitrile	II°	Water	HH
Chloroform	HH	Toluene	HH
Dichloromethane	HH	Xylene	HH
Dichloroethane	HH	Cyclohexane	HH, II°
Diethyl ether	II°	Cyclohexanone	II°
Diisopropyl ether	HH	Heptane	HH

^a β RA and few drops of solvent were grinded in a grinding mill (Retsch Schwingmuehle MM301) for 7.5 minutes.

Table S5. Results: Vapor diffusion experiments^a (II° – form II°, I - form I, HH – hemihydrate, S_{DMSO} – DMSO solvate, S_{AA} – acetic acid monosolvate, S_{DMF-II} – dimethyl formamide ¾ solvate).

Solvent	Description (HTM)	Form
<i>n</i> -Butanol	Needles and platy crystals	II°, I
<i>i</i> -Butanol	Rectangular plates	HH
<i>n</i> -Propanol	Rectangular plates	HH
<i>i</i> -Propanol	Needles and plates	II°, I
Ethanol	Needles	II°
Methanol	Needles	II°
Acetic acid	Needles	II°
Acetone	Needles	II°
Acetonitrile	Needles and plates	II°, I
Chloroform	Needles and few plates	II°, I
Diethyl ether	Needles and plates	II°, I
Disopropyl ether	Needles and plates	II°, I
Dioxane	Needles	II°
Dimethyl formamide	Solvate (platy)	S _{DMF-II}
Dimethyl sulphoxide	Needles	II°
Ethyl methyl ketone	Needles and plates	II°, I
Ethylacetate	Needles	II°
Nitromethane	Needles and plates	II°, I
Pyridine	yellow crystals	Pyridinium-Salt
Tetrahydrofurane	Needles	II°
Water	Rectangular plates	HH

^aA saturated solution of β RA was prepared at RT and placed in a small open vial, which was placed upright in a larger closed vial in which a quantity of anti-solvent had been added.

Solid-State Forms of β -Resorcylic Acid: How Exhaustive should a Polymorph Screen be?

1.2 Thermal analysis, thermodynamic and kinetic stability

Figure S1 shows the dehydration of β RA *HH* embedded in silicon oil.

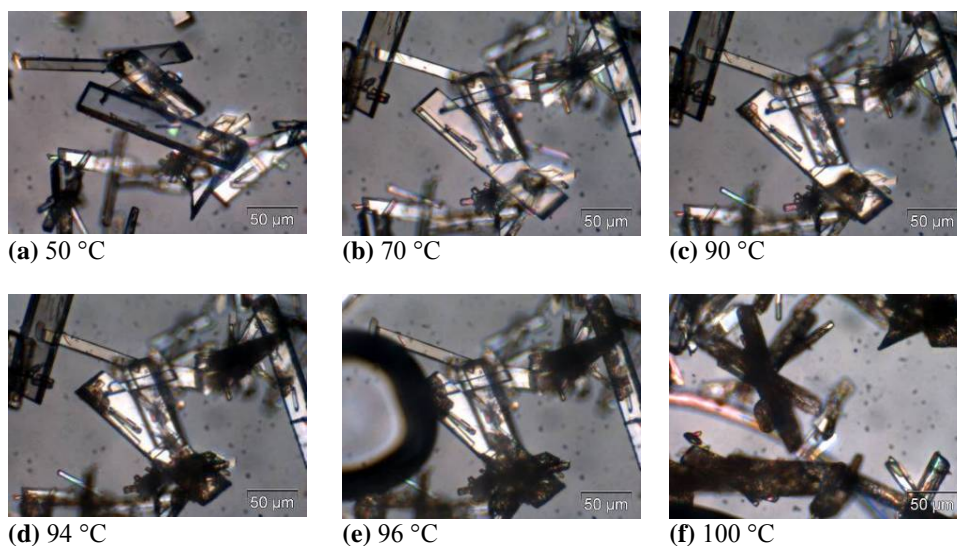


Figure S1. Photomicrographs (embedded in silicon oil) showing the dehydration process of β RA *HH*.

The thermodynamic relationship of the two β RA modifications is displayed in a semi-schematic energy/temperature diagram (Figure S2).^{1,2}

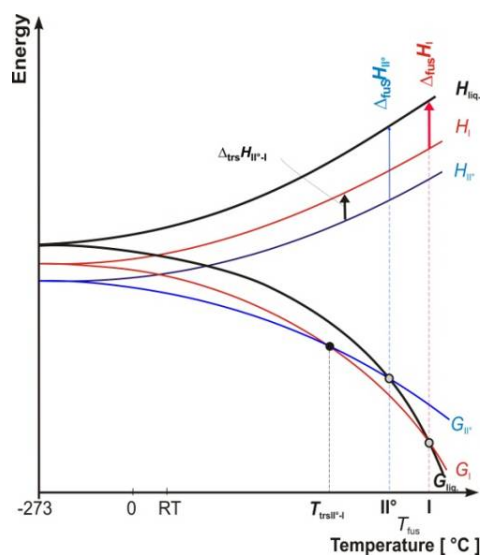


Figure S2. Semi-schematic energy/ temperature diagram of β RA polymorphs. T_{fus} : melting point, G : Gibbs free energy, H : enthalpy, $\Delta_{\text{fus}}H$: enthalpy of fusion, T_{trs} : transition point, $\Delta_{\text{trs}}H$: transition enthalpy, liq: liquid phase (melt).

1.3 X-ray diffractometry

1.3.1 Powder X-ray diffraction data for structure determination of form I

Table S6. Variable count time scheme for powder X-ray data collection used for form I structure determination.

2θ range ($^{\circ}$)	Count time (s per step)
3 to 22	2
22 to 40	5
40 to 55	12
55 to 70	24

1.3.2 Identification of β RA phases

The *powder X-ray diffraction patterns* (Figure S3, Table S7) were obtained using a X'Pert PRO diffractometer (PANalytical, Almelo, The Netherlands) equipped with a theta/theta coupled goniometer in transmission geometry, programmable XYZ stage with well plate holder, Cu-K $\alpha_{1,2}$ radiation source with a focussing mirror, a 0.5 $^{\circ}$ divergence slit and a 0.02 $^{\circ}$ Soller slit collimator on the incident beam side, a 2 mm antiscattering slit and a 0.02 $^{\circ}$ Soller slit collimator on the diffracted beam side and a solid state PIXcel detector. The patterns were recorded at a tube voltage of 40 kV, tube current of 40 mA, applying a step size of $2\theta = 0.013^{\circ}$ with 20 s or 40 s per step in the 2θ range between 2 $^{\circ}$ and 40 $^{\circ}$.

The mechanical instability of all β RA phases except form II $^{\circ}$ and *HH* allowed the samples only to be ground gently and variations in intensities in the powder patterns due to preferred orientation could not be prevented.

Solid-State Forms of β -Resorcylic Acid: How Exhaustive should a Polymorph Screen be?

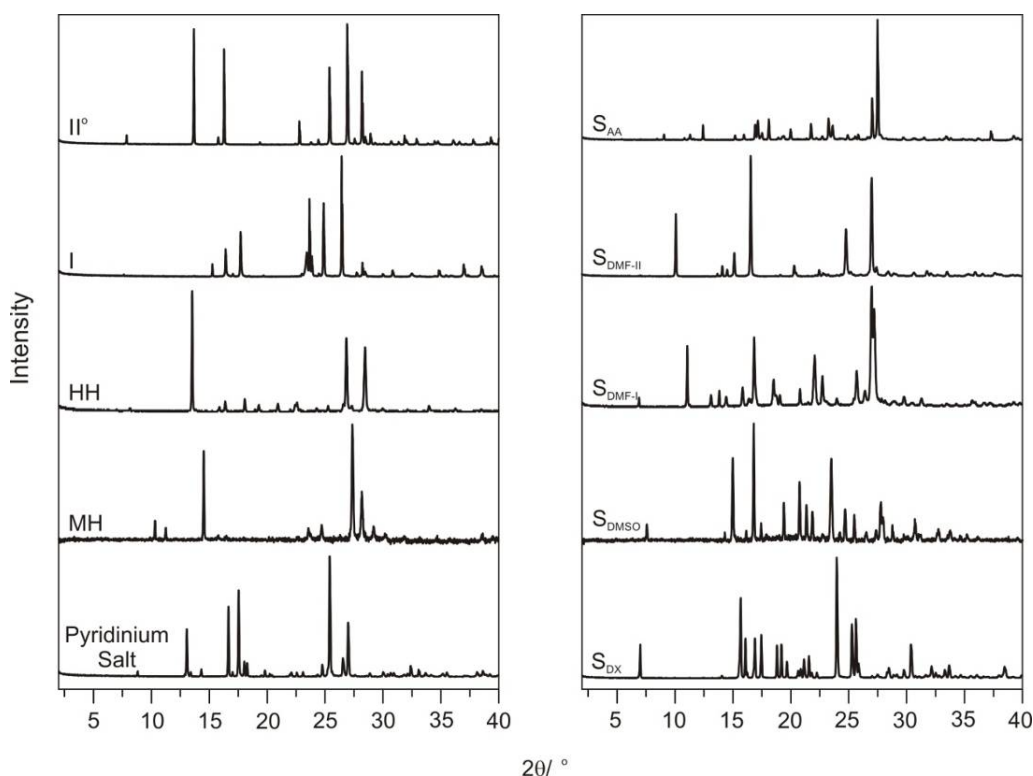


Figure S3. Powder X-ray diffraction patterns of the β RA polymorphs (I, II^o), hydrates (HH, MH), solvates (S_{AA}, S_{DMF-II}, S_{DMF-I}, S_{DMSO} and S_{DX}) and the pyridinium salt.

Table S7. Characteristic 2θ positions of the different β RA solid state forms and the pyridinium salt.

Form II ^o	Form I	HH	MH	S _{AC}	S _{DMF-II}	S _{DMF-I}	S _{DMSO}	S _{DX}	Pyridine
7.87	15.27	13.52	10.30	12.39	10.13	11.08	14.96	15.67	13.07
13.68	16.42	16.39	14.52	16.92	14.13	16.85	20.73	16.09	16.66
16.28	17.71	18.06	23.57	18.10	15.18	18.52	21.34	16.91	17.54
22.78	23.65	19.28	24.71	21.76	16.59	22.08	21.84	17.47	24.77
25.38	24.88	20.93	27.37	23.29	20.35	25.71	23.46	24.00	25.42
26.92	26.50	22.57	28.18	23.63	24.81	26.98	24.66	25.30	26.65
28.17	28.22	28.45	29.20	27.07	27.02	27.21	27.74	25.65	27.01
				27.53				30.40	

1.3.3 Variable temperature and moisture PXRD measurements

Temperature and moisture dependent measurements (Figure S4 and S5) were conducted on a Siemens D-5000 diffractometer equipped with a theta/theta goniometer, a Cu-K $\alpha_{1,2}$ radiation source, a Göbel mirror (Bruker AXS, D), a 0.15° Soller slit collimator and a scintillation counter, equipped with a low temperature chamber (TTK, Anton Paar, A)

Solid-State Forms of β -Resorcylic Acid: How Exhaustive should a Polymorph Screen be?

interfaced with a SETARAM-WETSYS humidity generator (KEP-technologies, USA) to control the relative humidity (RH) in the chamber. The patterns were recorded at a tube voltage of 40 kV and a tube current of 40 mA, applying a scan rate of $0.05^\circ 2\theta \text{ s}^{-1}$ in the angular range of 2 to $40^\circ 2\theta$.

HH dehydration was monitored at 0% relative humidity and RT. The dehydration led to a mixture of the two polymorphs. *MH* was monitored at ambient conditions (*ca.* 40% RH and RT) and resulted in pure form II^o. Scan number corresponds to time in the figures.

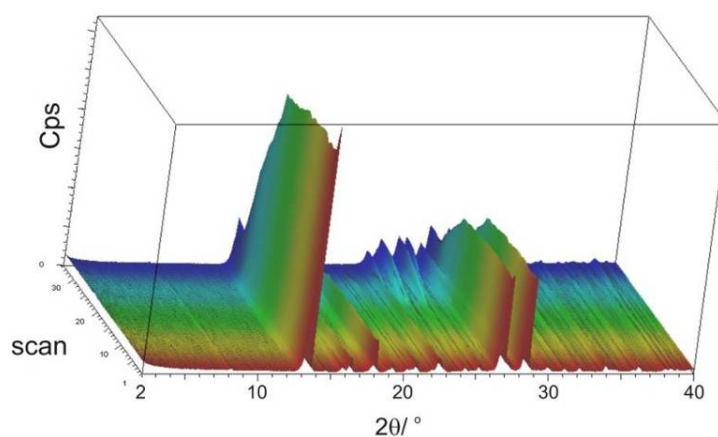


Figure S4. PXR D temperature-scan showing the dehydration of β RA *HH* (front – hemihydrate, back – form II^o and I) at RT and 0% RH. Time range: 5 days

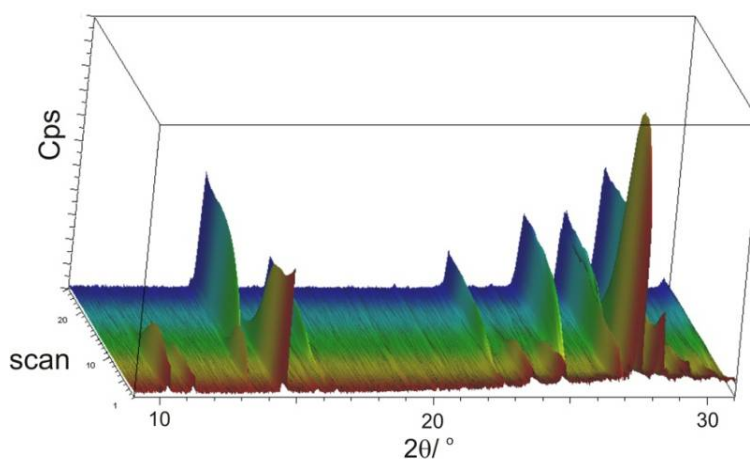


Figure S5 PXR D temperature-scan showing the dehydration of β RA *MH* in the range from 9 to 31 2θ recorded at ambient conditions (front – monohydrate, back – form II^o). Time range: 2 hours

Solid-State Forms of β -Resorcylic Acid: How Exhaustive should a Polymorph Screen be?

1.3.4 Pyridinium salt: hydrogen bonding motif

The pyridinium cation interacts with the β RA anion *via* an ionic $N^+ \cdots H \cdots O$ hydrogen bond. The anion forms a helix along *b*, mediated by 2_1 symmetry (Figure S6).

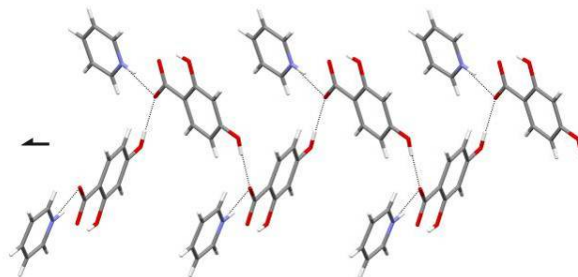


Figure S6. Hydrogen bonding motif present in the β RA pyridinium salt.

2 THEORETICAL

2.1 Conformational analysis of β RA and the choice of method for ΔE_{intra}

The conformational energy scans for isolated β RA given in Figure S7 show that there are eight distinct planar minima, separated by significant barriers. The *p*-OH group can rotate significantly for minimal energy cost, in agreement with the experimental conformations. The relative energies of the eight fully optimized conformations (Table S8) depend slightly on the level of theory, but there is a clear pattern of having pairs of conformations of similar energy differing in the orientation of the *p*-OH proton. There is a significant energy difference for swapping the position of the carboxylic acid proton and an even larger penalty of *ca.* 50 kJ mol⁻¹ for breaking the intramolecular hydrogen bond. The PBE0/6-31G(d,p) method was chosen to model ΔE_{intra} in the final lattice energy minimization (stage 3 ESI 2.4.1) as the best compromise between accuracy and computational cost.

The most stable crystal structures generated with each conformation show that the conformations without an intramolecular hydrogen bond can pack with an additional intermolecular hydrogen bond, but the improvement in the intermolecular lattice energy does not compensate for the loss of the intramolecular hydrogen bond (Table S8). Our lattice energy model may be incorrectly modeling the balance between intra- and intermolecular hydrogen bonds, as ΔE_{intra} was derived from isolated gas phase optimizations and is quite sensitive to the method of calculation.³ However the energy differences are so large that we can exclude the possibility of crystal structures without the intramolecular H-bond.

Solid-State Forms of β -Resorcylic Acid: How Exhaustive should a Polymorph Screen be?

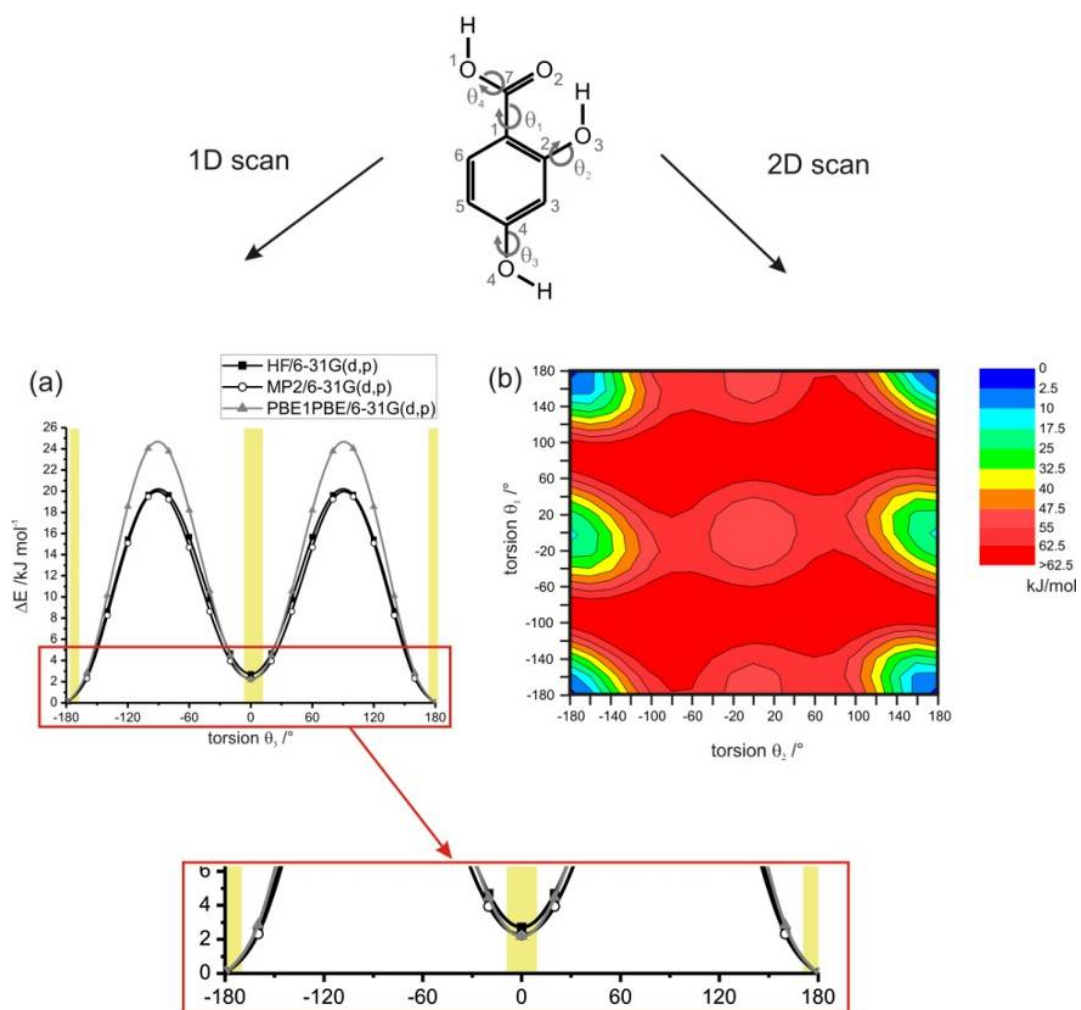


Figure S7. Potential energy surface scans for β RA with respect to (a) θ_3 (1D scan) and (b) θ_1 and θ_2 at the HF level of theory with the 6-31G(d,p) basis set. The range of experimentally observed torsion angles for the *p*-OH group is denoted on (a) with yellow bands.

Solid-State Forms of β -Resorcylic Acid: How Exhaustive should a Polymorph Screen be?

Table S8. β RA conformational energy minima and their ΔE_{intra} values with respect to the global conformational minimum (conf_p1); summary of rigid-body (stage 2) search results. E_{latt} : lattice energy, where E_{latt} = the sum of the intermolecular lattice energy (U_{inter}) and the conformational energy penalty (ΔE_{intra}).

Level of theory for calculating ΔE_{intra} / conformations	conf_p1	conf_p2	Conf_o_p1	Conf_o_p2
HF/6-31G(d,p) / kJ mol ⁻¹	0	2.72	50.96	48.44
MP2/6-31G(d,p) / kJ mol ⁻¹	0	2.27	50.30	47.69
PBE0/6-31G(d,p) / kJ mol ⁻¹	0	2.22	57.99	55.35
DMACRYS minima within 5/10 kJ mol ⁻¹ of overall global minimum	24/107	0/19	0/0	0/0
U_{inter} / kJ mol ⁻¹	-116.18	-112.28	-130.67	-132.37
E_{latt} (lowest), stage 2/ kJ mol ⁻¹	-116.18	-109.56	-71.71	-83.93
	conf_COOH_p1	conf_COOH_p2	conf_COOH_o_p1	conf_COOH_o_p2
HF/6-31G(d,p) / kJ mol ⁻¹	16.15	17.96	47.87	44.67
MP2/6-31G(d,p) / kJ mol ⁻¹	17.72	18.09	48.97	45.61
PBE0/6-31G(d,p) / kJ mol ⁻¹	19.51	20.81	55.12	51.88
DMACRYS minima within 5/10 kJ mol ⁻¹ of overall global minimum	0/0	0/0	0/0	4/201
U_{inter} / kJ mol ⁻¹	-121.43	-116.78	-130.97	-132.16
E_{latt} (lowest), stage 2/ kJ mol ⁻¹	-105.29	-98.82	-83.10	-87.49

2.2 Testing the model for the intermolecular forces for U_{inter}

The modeling of the intermolecular forces was tested by the reproduction of the crystal structures of form II^o, the hemihydrate and 19 related molecules (phenols, benzoic acid derivatives and their hydrates) chosen to also be single crystal determinations with the proton positions located from the Fourier difference maps. The subset of results for β RA form II^o and the hemihydrate (*HH*) are shown in Table S9. We considered various parameterizations of the atom-atom exp-6 repulsion-dispersion potential of the form:

$$U = \sum_{i \in 1, k \in 2} (A_{ii} A_{kk})^{1/2} \exp(-(B_{ii} + B_{kk})R_{ik} / 2) - \frac{(C_{ii} C_{kk})^{1/2}}{R_{ik}^6}$$

where atom i in molecule 1 is of type ι and separated by R_{ik} from atom k , of type κ , in molecule 2. The various sets of parameters were tested in conjunction with an MP2/6-31G(d,p) distributed multipole model for the electrostatic contribution.

The use of the recent Williams parameterization⁴ (**W01**) gave very short intermolecular hydrogen bonds in the carboxylic acid $R_2^2(8)$ dimers. The older **FIT**⁵⁻⁷ parameterization, in contrast resulted in these hydrogen bonds being somewhat too long in a number of the structures. An attempt to improve this by modifying (**FIT**_{COOH}) the pre-exponential term A_{ii} for the polar hydrogen in the COOH group, gave an excellent reproduction of all hydrogen bond lengths with an optimized value of 3018 kJ mol⁻¹ (compared to 5030 kJ mol⁻¹ in the FIT parameterization).

Since the **FIT**_{COOH} used in conjunction with the MP2/6-31G(d,p) distributed multipoles appeared to satisfactorily reproduce the large set of crystal structures, it was used initially in stage 2 of the search. Although this found form II^o of β RA, it was ca. 5 kJ mol⁻¹ above the global lattice energy minimum. This search also found a chain (ch) structure (Figure 13) that is not observed at all in the CSD as the global minimum and in the majority of low energy crystal structures. This prompted an investigation into the sensitivity of the intermolecular potential to the charge density used to define the electrostatic contribution to the lattice energy.

The electrostatic potential around β RA in the two lowest energy conformations, as calculated from the distributed multipoles shows marked differences (Figure S8) when calculated from the MP2/6-31G(d,p) or PBE0/aug-cc-pVTZ charge densities. There is a clear difference in that the carbonyl oxygen region becomes more negative and the *p*-OH oxygen region less negative with the better PBE0/aug-cc-pVTZ charge density. This resulted in a change in the favorability of the different hydrogen bonding motifs.

Solid-State Forms of β -Resorcylic Acid: How Exhaustive should a Polymorph Screen be?

Thus the final model (**FINAL**) used in the stage 2 and 3 for the lattice energy landscapes (Figure 13, Tables S9 - S12) used the FIT parameters and the distributed multipole of the PBE0/aug-cc-pVTZ charge density. This gave satisfactory reproduction of 14 carboxylic acid structures, in addition to those of β RA shown in Table S9.

Table S9. The reproduction of experimental β RA crystal structures following stage 3 minimization of $E_{\text{latt}} = U_{\text{inter}} + \Delta E_{\text{intra}}$ using different repulsion-dispersion potential parameters and ab initio charge densities.

potential	Lattice parameters (cell vectors/Å, angles/°) ($\Delta/\text{Å}, ^\circ$)						cell density g/cm ³ ($\Delta/\%$) ^e	rmsd ₁₅ ^f (Å)
	<i>a</i>	<i>b</i>	<i>c</i>	α	β	γ		
Form A ^o (ZZZEEU03)								
Expt ^a	3.674	22.341	8.007	90	99.57	90	1.580	
W01 ^b	(0.139)	(-0.124)	(-0.157)		(3.02)		(-0.148)	0.280
FIT ^b	(0.050)	(0.447)	(-0.154)		(2.88)		(-0.410)	0.261
FIT _{COOH} ^c	(0.078)	(0.257)	(-0.171)		(3.00)		(-0.063)	0.221
FINAL ^d	(0.089)	(0.040)	(0.032)		(1.93)		(-2.33)	0.158
Hemihydrate (QIVTUK)								
Expt ^a	7.026	9.547	11.199	96.78	104.34	98.85	1.527	
FIT _{COOH} ^c	(-0.165)	(-2.686)	(-0.105)	(-1.25)	(2.36)	(0.89)	(2.13)	0.220
FINAL ^d	(-0.072)	(0.337)	(-0.272)	(-2.29)	(1.27)	(2.82)	(1.16)	0.237

^aThe experimental structures (expt) are compared with the minimum in the lattice energy found for the conformationally relaxed structure (stage 3), using the ^{b,c}MP2/6-31G(d,p) or ^dPBE0/aug-cc-pVTZ for DMA + exp-6 potential and the ^{b,d}FIT/ ^cmodified FIT repulsion-dispersion parameters and ΔE_{intra} derived from ^{b,c}HF/6-31G(d,p) or ^dPBE0/6-31G(d,p). ^eQuantities in parentheses are percentage error, $\Delta/\% = 100((\text{stage3} - \text{expt})/\text{expt})$. ^fThe quality of the reproduction of the crystal structures was evaluated by the optimal root-mean square overlay of all non-hydrogen atoms and non-water molecules in a 15 molecule coordination cluster (rmsd₁₅).

Solid-State Forms of β -Resorcylic Acid: How Exhaustive should a Polymorph Screen be?

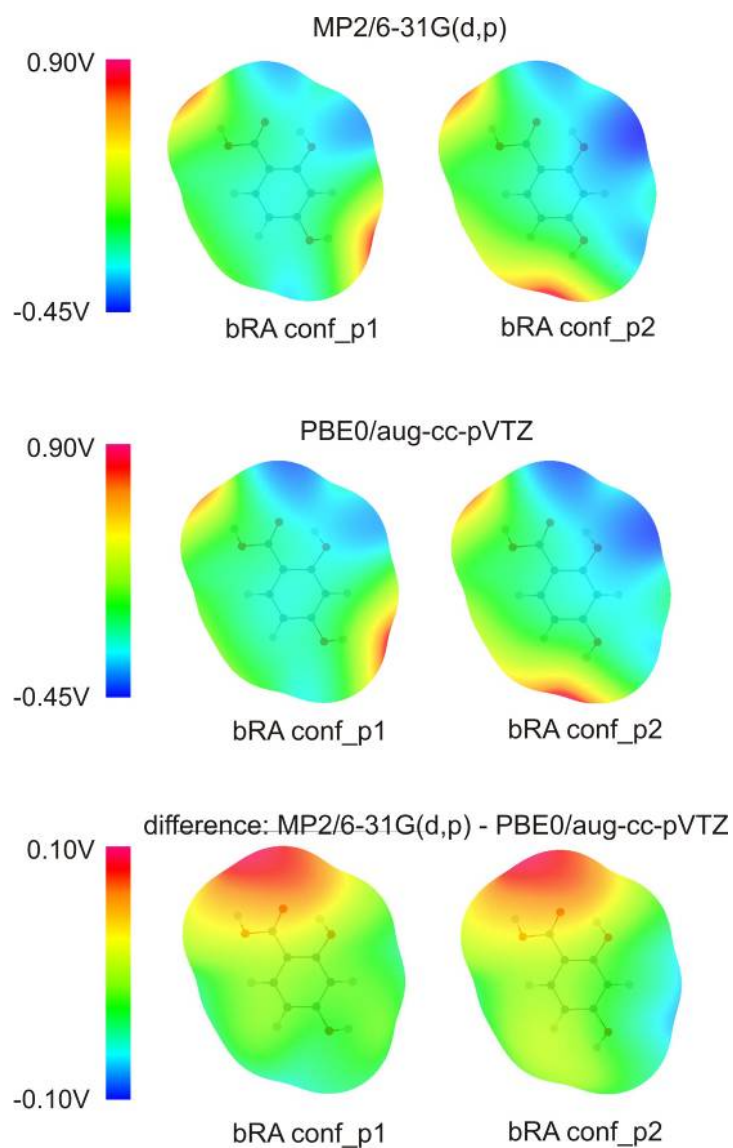


Figure S8. Electrostatic potential (V) maps for β RA on a surface defined by twice the atomic van der Waals radii calculated from the distributed multipoles of the MP2/6-31G(d,p) and PBE0/aug-cc-pVTZ molecular charge densities for conf_p1 and conf_p2, drawn with ORIENT.⁸ The van der waals radii were those of Bondi,⁹ except there was an effectively zero radius for polar hydrogen atoms to reflect the close distances in hydrogen bonds.

2.3 Modeling of form I

The final computational model was successful in modeling all well-determined experimental crystal structures and produced a plausible lattice energy landscape. However, modeling of the anhydrous form I gave significant errors (Table S10). The lattice energy minima predicted that the anhydrous form I was denser than form II^o, in marked contrast to the observed and usual situation where the high temperature form is less dense. The lattice energy minima nominally correspond to static 0 K structures, but the empirical parameterization of the FIT potential to crystal structures implies that some thermal effects have been absorbed. Contrasting the experimental structures for form II^o and *HH* at a range of temperatures (Table S10), shows normal thermal expansion, and that the potential is slightly underestimating the density for II^o. Hence the 6% overestimate of the density of form I is not due to normal thermal expansion effects.

Table S10. Experimentally measured temperature dependent change of lattice parameters and densities for form II^o and *HH*, along with the quality of representation of the crystal structures.

	Lattice parameters (cell vectors/Å, angles ^o)						cell density	
	<i>a</i>	<i>b</i>	<i>c</i>	α	β	γ	g cm ⁻³	$\Delta/\%$ ^a
Form II ^{ob}								
Stage 3	3.763	22.381	8.170		105.35		1.543	
20K ¹⁰	3.656	22.329	8.221		106.23		1.589	-2.90
90K ¹¹	3.669	22.333	8.229		106.45		1.583	-2.53
90K ¹⁰	3.669	22.347	8.235		106.43		1.581	-2.40
100K ¹¹	3.672	22.341	8.233		106.49		1.581	-2.40
110K ¹¹	3.672	22.341	8.236		106.53		1.580	-2.34
150K ¹¹	3.685	22.367	8.248		106.71		1.572	-1.85
150K ¹⁰	3.686	22.368	8.254		106.70		1.571	-1.78
Hemihydrate								
Stage 3	6.954	9.884	10.927	94.49	105.61	101.67	1.545	
173K	7.027	9.545	11.176	96.68	104.32	98.90	1.530	+0.98
RT	7.026	9.547	11.199	96.78	104.34	98.85	1.527	+1.18
Form I								
Stage 3	20.872	4.993	6.057		92.96		1.624	
298K	23.198	5.547	5.198		92.22		1.532	+6.01

^a $\Delta/\%$ = 100*(Stage 3 – experimental)/experimental; ^bexperimental crystal structures transformed to $P2_1/c$ using Powder Cell.¹²

We computationally generated three alternative ordered versions of form I differing only in the proton positions which were kept fixed: two $Z'=1$ with the *p*-OH proton pointing either to the *o*-OH oxygen or the *p*-OH oxygen of an adjacent β RA molecule and a $Z'=2$ structure, *Pc*, with one *p*-OH proton pointing to the *o*-OH oxygen and the second to the *p*-OH oxygen. Table S11 gives detailed results for the anhydrate modeling, including the computational investigations of proton disorder in form I. The lattice energies for the alternative form I

Solid-State Forms of β -Resorcylic Acid: How Exhaustive should a Polymorph Screen be?

structures were *ca.* 8 kJ mol⁻¹ less stable than these for the experimental proton position. The lower stability can be attributed mainly to the less favorable β RA conformation (ΔE_{intra} contribution) c.f. Figure S7a. Allowing a change in conformation in these alternative crystal structures (stage 3) led to the same computational minima independent of where the *p*-OH proton was initially pointing. It has to be noted that we could not have found the alternative form I structures in our rigid-body searches (step 2) as we did not consider these conformations as rigid-body input conformations.

Solid-State Forms of β -Resorcylic Acid: How Exhaustive should a Polymorph Screen be?

Table S11. Computational modeling of β RA forms II^o and I.

	a/Å	b/Å	c/Å	β ^o	Density /g cm ⁻³	θ_3 ^o	O4...O4 /Å	O4...O3 /Å	rmsd ₁₅ ^c	U_{inter} /kJ mol ⁻¹	ΔE_{intra} /kJ mol ⁻¹	E_{latt} /kJ mol ⁻¹	ZPE ^d /kJ mol ⁻¹	Total thermal Energy	Free energy at 289K ^e /kJ mol ⁻¹
Form II ^o															
Exp. ^a	3.656	22.329	8.221	106.23	1.589	-	-	-	-	-	-	-	-	-	-
Stage 2 ^b	3.782	22.317	8.233	106.20	1.532	-	-	-	0.169	-114.20	0	-114.20	3.06	-17.97	-129.11
Stage 3	3.763	22.381	8.170	105.35	1.543	-	-	-	0.162	-115.46	0.65	-114.81	3.10	-17.85	-129.56
Form I															
Exp. ^a	5.198	5.547	23.198	92.21	1.532	180	3.244	2.827	-	-	-	-	-	-	-
Stage 2 ^b	5.868	5.072	21.428	93.50	1.608	180	2.947	2.931	0.873	-115.36	0	-115.36	3.24	-17.30	-129.42
RB ^b pointing to o-OH	5.396	5.492	22.049	97.34	1.580	151	3.175	2.839	0.539	-116.13	6.81	-109.32	3.12	-18.00	-124.20
RB ^b pointing to p-OH	6.167	4.837	21.701	90.17	1.582	-151	2.843	3.009	1.089	-114.75	6.76	-107.99	3.27	-17.38	-122.10
Z ² =2 ^b	5.405	5.457	22.216	95.82	1.571	151/-	2.980/ 2.980	2.792/ 2.936	0.567	-112.19	4.89	-107.30	3.09	-18.31	-122.52
stage 3	6.057	4.993	20.872	92.96	1.624	-178	2.930	2.952	1.063	-116.93	0.79	-116.14	3.34	-16.95	-129.75

^aexperimental crystal structures transformed to $P2_1/c$ using Powder Cell.¹² ^bRigid-body minimizations. ^cThe quality of the reproduction of the crystal structures was evaluated by the optimal root-mean square overlay of all non-hydrogen atoms in a 15 molecule coordination cluster (rmsd₁₅). ^dzero-point energy. ^eThe Helmholtz free energy as estimated from the lattice energy, zero point intermolecular energy, and temperature dependence of the rigid molecule internal energy and entropy, as derived from the $k=0$ second derivative properties.¹³

2.4 Computational generation of the crystal energy landscape (CSP)

2.4.1 Methodology (additional information)

Stage 1 $Z' = 1$ and $Z' = 2$ crystal structures were generated (Crystal Predictor) in the following 25 space groups: $P1$, $P-1$, $P2_1$, $P2_1/c$, $P2_12_12$, $P2_12_12_1$, $Pna2_1$, $Pca2_1$, $Pbca$, $Pbcn$, $C2/c$, Cc , $C2$, Pc , Cm , $P2_1/m$, $C2/m$, $P2/c$, $C222_1$, $Pmn2_1$, $Pnna$, $Pccn$, $Pbcm$, $Pmmn$, and $Pnma$. For the $Z'=1$ structures all planar conformational minima (Table S8) were used. In addition $Z' = 2$ structures containing the global (conf_p1) and second lowest (conf_p2) energy conformational minima in the asymmetric unit were generated. The molecules were held rigid in their HF/6-31G(d,p) optimized conformations. The model for the intermolecular forces used the FIT^{6,7,14} potential with modified A_{ii} for the carboxylic acid proton, 3018 kJ mol⁻¹, and the atomic charges fitted to the MP2(fc)/6-31G(d,p) electrostatic potential using the CHELPG scheme.¹⁵

Stage 2 All crystallographically distinct, $Z'=1$ generated crystal structures within 20 kJ mol⁻¹ from the corresponding search minimum (289 to 1822 structures) and the 7500 most stable unique $Z'=2$ structures (11.04 kJ mol⁻¹ energy range) were reminimized. The intermolecular lattice energy was calculated using the FIT^{6,7,14} *exp-6* potential parameters and the distributed multipoles¹⁶ up to hexadecapole derived from the PBE0/aug-cc-pVTZ charge density using GDMA2.¹⁷ Conformations were kept rigid at the HF/6-31G(d,p) optimized geometries.

Stage 3 In the *final stage* (CrystalOptimizer) the four flexible torsion angles shown in Figure 1 were minimized as a response to the packing forces, in addition to the cell geometry and relative position and orientation of all molecules in the lattice. All other intramolecular degrees of freedom were allowed to relax to their isolated molecule optimized values for the corresponding values of the flexible torsions. This was done by using CrystalOptimizer¹⁸ by minimizing the lattice energy (E_{latt}), calculated as the sum of the intermolecular contribution (U_{inter}) and the conformational energy penalty (ΔE_{intra} , with respect to the global conformational minimum) paid to improve the intermolecular interactions. Conformational energy penalties and isolated-molecule charge densities were computed at the PBE0/6-31G(d,p) and PBE0/aug-cc-pVTZ levels, respectively, in the on-the-fly quantum-mechanical calculations.

2.4.2 The Crystal Energy Landscape following relaxation of the conformation within the crystal structure (stage 3)

The hypothetical crystal structures are available in *.res from the authors on request.

Table S12. Structurally Characterized and Hypothetical Low-energy Crystal Structures of β RA.

Structure ^a	Space group	Reduced cell parameters						$E_{\text{latt}}/\text{kJ mol}^{-1}$	Density/ g cm^{-3}
		a/Å	b/Å	c/Å	$\alpha/^\circ$	$\beta/^\circ$	$\gamma/^\circ$		
Experimentally observed Anhydrates minimized with CrystalOptimizer									
Π^{oa}	$P2_1/c$	3.763	22.381	8.170	90	105.347	90	-114.81	1.543
I^a	$P2_1/c$	6.057	4.994	20.872	90	92.964	90	-116.14	1.624
Anhydrate Search 1: $Z'' = 1$, conf_p1									
1_A7	$P2_1/c$	6.054	4.994	20.879	90	92.964	90	-116.14	1.624
1_A573	$P2_1/c$	12.353	3.774	4.976	90	114.135	90	-116.11	1.607
1_A1	$P2_1/c$	8.626	5.141	14.279	90	93.321	90	-116.06	1.619
1_A53	$P2_1/c$	6.667	8.866	10.887	90	101.183	90	-115.78	1.621
1_A17	$P2_1/c$	6.981	3.788	24.424	90	100.163	90	-115.12	1.610
1_A1151	$P2_1/c$	6.895	3.786	25.193	90	105.262	90	-114.90	1.614
1_A540	$P2_1/c$	3.762	22.398	8.157	90	105.260	90	-114.83	1.544
1_A18	$P2_1/c$	3.708	7.719	23.150	90	95.175	90	-114.50	1.551
1_A4	$P2_1/c$	11.482	3.726	16.635	90	118.707	90	-114.49	1.640
1_A2	$P2_1/c$	10.450	3.762	16.550	90	105.646	90	-114.44	1.634
1_A82	$P2_1/c$	4.182	6.780	24.230	90	99.312	90	-114.0	1.510
1_A5	$P2_1/c$	10.446	3.671	16.734	90	104.206	90	-114.14	1.645
1_A39	$P2_1/c$	11.093	3.911	15.109	90	103.365	90	-113.77	1.605
1_A45	$C2/c$	25.931	3.843	13.314	90	108.209	90	-113.53	1.624
1_A224	$P2_1/c$	11.673	3.676	16.709	90	119.672	90	-113.32	1.643
1_A33	$P2_1/c$	8.571	7.917	9.838	90	95.634	90	-113.32	1.541
1_A3	$P2_1/c$	11.673	3.676	16.708	90	119.663	90	-113.31	1.643
1_A157	$Pbca$	16.635	20.312	3.721	90	90	90	-113.25	1.630
1_A8	$P2_1/c$	8.415	5.203	14.573	90	100.072	90	-113.07	1.629
1_A9	$P2_1/c$	8.415	5.203	14.576	90	100.074	90	-113.05	1.630
1_A126	$Pbca$	3.703	16.692	20.326	90	90	90	-112.78	1.629
1_A193	$C2/c$	24.922	4.322	12.178	90	97.924	90	-112.76	1.576
1_A120	$C2/c$	16.165	9.178	10.633	90	119.746	90	-112.70	1.495
1_A52	$P2_12_12_1$	7.049	8.718	10.419	90	90	90	-111.84	1.599
Anhydrate Search 3: $Z'' = 2$, conf_p1 and conf_p2									
12_A3	$P-1$	5.249	8.505	14.097	91.436	90	90	-113.82	1.627
12_A4	$P2_1/c$	8.510	5.2452	14.110	90	91.644	90	-113.80	1.626
12_A2	$P2_1/c$	10.450	3.762	16.550	90	105.646	90	-113.72	1.627
12_A91	$P-1$	4.930	6.278	21.347	88.300	88.535	78.056	-113.28	1.585

^aexperimental structures transformed to conventional setting using PLATON.¹⁹ Labels for hypothetical structures correspond to internal res file names, are of format conformation_search output name. The structures found in the search which correspond to the known forms are in bold text.

Solid-State Forms of β -Resorcylic Acid: How Exhaustive should a Polymorph Screen be?

Reference List

1. Burger, A.; Ramberger, R. *Mikrochimica Acta* **1979**, *2*, 259-271.
2. Burger, A.; Ramberger, R. *Mikrochimica Acta* **1979**, *2*, 273-316.
3. Karamertzanis, P. G.; Day, G. M.; Welch, G. W. A.; Kendrick, J.; Leusen, F. J. J.; Neumann, M. A.; Price, S. L. *J.Chem.Phys.* **2008**, *128*, art-244708.
4. Williams, D. E. *J.Comput.Chem.* **2001**, *22*, 1154-1166.
5. Coombes, D. S.; Price, S. L.; Willock, D. J.; Leslie, M. *J.Phys.Chem.* **1996**, *100*, 7352-7360.
6. Williams, D. E.; Cox, S. R. *Acta Crystallogr., Sect.B* **1984**, *40*, 404-417.
7. Cox, S. R.; Hsu, L. Y.; Williams, D. E. *Acta Crystallogr., Sect.A* **1981**, *37*, 293-301.
8. *ORIENT: a program for studying interactions between molecules*, version 4.6; Stone, A. J.; Dullweber, A.; Engkvist, O.; Fraschini, E.; Hodges, M. P.; Meredith, A. W.; Nutt, D. R.; Popelier, P. L. A.; Wales, D. J. University of Cambridge, **2006**
9. Bondi, A. *J.Phys.Chem.* **1964**, *68*, 441-451.
10. Adam, M. S.; Gutmann, M. J.; Leech, C. K.; Middlemiss, D. S.; Parkin, A.; Thomas, L. H.; Wilson, C. C. *New J.Chem.* **2010**, *34*, 85-91.
11. Parkin, A.; Adam, M.; Cooper, R. I.; Middlemiss, D. S.; Wilson, C. C. *Acta Crystallographica, Section B: Structural Science* **2007**, *B63*, 303-308.
12. Kraus, W.; Nolze, G. *J.Appl.Crystallogr.* **1996**, *29*, 301-303.
13. Price, S. L.; Leslie, M.; Welch, G. W. A.; Habgood, M.; Price, L. S.; Karamertzanis, P. G.; Day, G. M. *Phys.Chem.Chem.Phys.* **2010**, *12*, 8478-8490.
14. Coombes, D. S. *Philos.Mag.B* **1996**, *73*, 117-125.
15. Breneman, C. M.; Wiberg, K. B. *J.Comput.Chem.* **1990**, *11*, 361-373.
16. Stone, A. J. *J.Chem.Theory Comput.* **2005**, *1*, 1128-1132.
17. *GDMA: A Program for Performing Distributed Multipole Analysis of Wave Functions Calculated Using the Gaussian Program System*, version 1.0; Stone, A. J. University of Cambridge: Cambridge, United Kingdom, **1999**
18. Kazantsev, A. V.; Karamertzanis, P. G.; Adjiman, C. S.; Pantelides, C. C. In *Molecular System Engineering*, Adjiman, C. S., Galindo, A., Eds.; WILEY-VCH Verlag GmbH & Co.: Weinheim, **2010**; 1-42.
19. *PLATON, A Multipurpose Crystallographic Tool*, Spek, A. L. Utrecht University: Utrecht, The Netherlands, **2003**